XVI International Conference on Durability of Building Materials and Components
DBMC 2023, China
K.F. Li and D.P. Fang (Eds)

Influence of Waste Fibers on the Total Porosity of Cementitious Composites

Katarina Didulica[1], Alenka Mauko Pranjić[2], Mateja Štefančić[2], Branka Mrduljaš[1] and Ana Baričević[1]

[1]Department of Materials, University of Zagreb, Zagreb 10 001, Croatia, kdidulica@grad.hr (KD (Corresponding author)), bmrduljas@grad.hr (BM), abaricevic@grad.hr (AB)

[2]Slovenian National Building and Civil Engineering Institute - ZAG, The Department of Materials, Slovenia, alenka.mauko@zag.si (AMP), mateja.stefancic@zag.si (MŠ)

Abstract. T*he amount of water is essential to explain the shrinkage process. It is determined by the water-cement ratio, but also by the moisture content. Water in hydrated cement paste occurs in various forms: chemically bound, interlayer, adsorbed, free water and water vapor. During cement hydration, the balance between various forms of water changes. For example, the amount of physically bound water diminishes, and the moisture content changes at similar environmental conditions. Moisture changes occur first in the larger pores and then in the smaller pores. The air pores are larger than the hydration pores (capillary pores, gel pores) and have a greater effect on strength and permeability properties, while the cement hydration pores have a greater effect on shrinkage. At early ages, when composite properties are not fully developed, higher shrinkage influences the development and propagation of cracks. These (micro)cracks represent weak points and affect durability. To reduce shrinkage and bridge the cracks, fibers are added to the cementitious composite. Depending on the type and geometry, the fibers can reduce shrinkage and bridge the cracks. To reduce the environmental impact of fiber production, the use of waste fibers in cementitious composites is proposed.*

The main objective of this study was to investigate the influence of alkali-resistant glass fibers from production waste on the development of the microstructure of cementitious composites, i.e., the influence on the total porosity. The pore content was determined on fresh cementitious composites after mixing, while the total porosity of the material was measured after 28 days using a mercury intrusion porosimeter. Results were complemented by X-ray computed microtomography (micro-CT). The influence of production waste fibers is presented as a function of length and fiber content. In addition to the reference mixture, results were also compared with mixtures containing factory-produced fibers.

Keywords: *Waste fibers; Air content; Total porosity; Mercury intrusion porosimeter; X-ray computed microtomography*

1 Introduction

Cementitious materials with high performance have overcome the shortcomings of ordinary cementitious materials and further promoted their use. The main changes concern composition, additions and curing conditions. In this way, stronger and more durable materials are obtained, but with an amplification of certain negative aspects, such as shrinkage and resulting cracks, which were not previously present to this extent. This is due to the finer aggregate, better particle packing and lower porosity with higher density achieved with more binder and less water (Shi et al., 2015; Wang et al., 2015). However, regardless of the packing degree, hardened cementitious composites always contain pores that play an important role in their properties.

Some of these pores are desirable and are obtained with chemical additives according to the requirements, but others are unavoidable and are formed during the hydration process and mixing. In both cases, the shape of the pores, their size and distribution affect the macroscopic mechanical behavior and durability of the hardened material. In addition, the pores may be empty or partially and fully saturated, which also affects the microstructure and volume deformations. The most common classification of pores is by size: gel pores (1 – 10 nm), capillary pores (10 – 10^4 nm), entrained air pores (10^4 - 10^6 nm) and entrapped air pores (10^6 – $5 \cdot 10^6$ nm). Entrained and entrapped pores are larger and thus affect strength and permeability, while gel and capillary pores affect shrinkage (Yu et al., 2021).

The hydration process in cementitious composites is characterized by the consumption of water, which leads to the formation of hydration products that gain strength by forming a rigid but porous structure. Fresh mortar under atmospheric pressure behaves like a dense suspension of inert aggregates and entrapped air bubbles embedded in a deformable matrix of cement paste (Craipeau et al., 2021). From the mixing to setting, volume changes occur and continue throughout the hydration. Shrinkage consists of hydration contraction, i.e., chemical shrinkage, and measured contraction i.e., autogenous, thermal, and drying shrinkage. Chemical shrinkage is a phenomenon that leads to the formation of pores during the hydration process due to the higher density of the hydration products compared to the raw materials (Wu et al., 2017). It is more pronounced in high properties materials due to the higher binder and lower water content. Such compositional changes result in microstructure densification and less influence of external curing, as it is difficult for the water to penetrate the central part. In such a structure, the self-desiccation in the pores is increased. In other words, drying shrinkage is reduced, but autogenous shrinkage is emphasized, so it is necessary to develop techniques to reduce autogenous shrinkage at early age. In recent years, various techniques have been explored to reduce shrinkage, acting on the different shrinkage forces (Tran et al., 2021; Yang et al., 2019). One of these techniques is the use of fibers. Their effect on shrinkage is defined as internal curing or restraint, where the fibers can overcome tensile stresses before cracks occur (delayed cracking) and bridge the crack after it has occurred (reducing the size and width of the crack).

Fibers can be used variously, but their impact on the composite is largely determined by the type and geometry. In addition to factory-produced fibers, waste fibers are increasingly being used due to favorable environmental and economic opportunities. One such valuable waste is alkali resistant glass fibers obtained during the manufacture of technical textiles. This type of waste is classified as clean waste i.e., waste that does not reach the end user but is separated at the factory for disposal. This material is not exposed to high temperatures and pressures, but only to the weaving machine, and it is considered that the mechanical properties do not deteriorate significantly, but surface scratches occur.

In order to explain the influence of waste glass fibers on the shrinkage properties of mortars, it is necessary to determine their influence on the microstructure i.e., the distribution and size of the pores. In this paper, the pore content was determined on fresh cementitious composites immediately after mixing, while the total porosity of the material was measured after 28 days using a mercury intrusion porosimeter (MIP) complemented by X-ray computed microtomography (micro-CT). The effect of alkali resistant glass production waste fibers (wGF) is shown as a function of length and fiber content. In addition to the reference mix (REF) without fibers, the results were also compared with mixes containing factory-made alkali resistant glass fibers (fGF).

2 Materials and Methods

Cement CEM I 52.5 N, aggregates, water, and superplasticizer Master Glenium® ACE 430 were used for the mortars tested. The aggregate consisted of the following fractions: limestone filler 0.005/ 0.125 mm, quartz sand 0/ 1.0 mm and dolomite fractions 0.1/ 0.6 mm, 0.6/ 1.25 mm and 1.25/ 2.0 mm. The water/ binder ratio was kept constant at 0.4, while the superplasticizer was increased depending on the amount of fibers. The superplasticizer used is a second generation polycarboxylic ether polymer-based admixture with high early strength gains. In this work, alkali-resistant waste glass fibers and factory- made glass fibers with the properties given in Table 1 were used. Alkali-resistant waste glass fibers are free of impurities and do not require cleaning, but preparation in the form of cutting with knives at 5 and 10 mm spacing was necessary. A total of five mixtures were prepared with the designation wGF and fGF for waste or factory- made glass fibers respectively, and a number indicating the length (5 or 10 and 6 or 12) followed by a number indicating the volume fraction of the fibers used (0.2 and 0.6 %V).

Table 1. Alkali resistant glass fibre properties.

Fibre ID	Trade name	Density [g/cm^3]	Diameter [µm]	Surface coating [%]
wGF	CEM-FIL® 5325, 1200 Owens Corning	2.68	14 - 24	~ 1.0
fGF	Schwarzwälder Textil-Werke	2.68	14	0.8

All powdered materials were first mixed with fibers in the dry state to improve dispersion using a professional shaker, subjected to high-frequency vibrations for 3 to 5 minutes, depending on the fiber content. During the mixing process, superplasticizer and water were added first followed by the dry mix. For the reference mix, the total mixing time was 4.5 minutes, of which 1 minute was mixed at the first speed, then a 1.5-minute break, followed by 2 minutes of mixing at the second speed. The same procedure was followed for the other mixes, with the only difference being that the initial mixing at the first speed was extended to 2 minutes due to insufficient dispersion of the fiber in the wGF10-6 mix.

Immediately after mixing, the properties were tested in the fresh state: density, temperature, air content, and consistency. Samples for hardened state properties testing were stored under laboratory conditions for 24 hours and then in a humid chamber for up to 28 days. The age of 28 days was chosen because no relevant change in pore morphology was expected thereafter. The cylinder specimens with a diameter of 8 mm to be further tested were drilled from prisms of 4 x 4 x 16 cm. Hydration was stopped by immersing the specimens in isopropanol for 7 days followed by vacuum drying for another 7 days. Specimens were then tested or stored in a nitrogen chamber to prevent carbonation.

Mercury intrusion porosimetry (MIP) was tested using AutoPore IV 9500 Micromeritics. The size of the pores that can be detected ranges from 2 nm to 1 mm. When interpreting the results, it should be taken into account that this method can only detect connected pores that can be reached with mercury under pressure. The MIP was performed on two samples and the mean values were shown. The mass of the test samples was approx. 1.45 g.

A microXCT-400 X-ray computed microtomograph (XRadia, Zeiss) was used. The device is designed for tomographic imaging of various inorganic and biological samples. It can be used

for analysis of both homogeneous and inhomogeneous materials. After the cylindrical specimen is placed and attached to the stand, which rotates 360°, the parameters used to image the specimens are set. The parameters used for recording specimens are: 40x magnification, source voltage 80 kV, power 10 W, exposure time 10 s. In this case, the distance from the X-ray source is 40 mm and the distance from the detector is 300 mm. The sample rotates 360° around its axis, and during the rotation of the sample, a total of 1801 images were acquired, which means that the device acquired an image every 0.33°. The minimum voxel size was 7.95.

3 Results and Discussion

3.1 Fresh state properties

The properties in the fresh state are given in **Table *2***, together with the amount of superplasticizer required to obtain values of the same category for plastic consistency, from 140 to 200 mm. The higher superplasticizer requirement, i.e. lower consistency values, with increase in fiber content was also found in previous work on concrete mixes (Ahmad et al., 2022; Blazy et al., 2022) and mortar mixes (Małek et al., 2021).

From the results, it can be seen that the density values using fGF differ only insignificantly from those of the reference mix (up to ± 0.5 %), while the influence of wGF becomes more evident with increasing fiber content. The values are 2.85 % and 7.91 % lower for 5 mm and 10 mm fibers, respectively. A higher proportion of wGF resulted in a reduction in the amount of aggregate and an increase in mixing time, as well as more entrapped air leading to the changes in density (da Silva & Lordsleem, 2021).

Air content values obtained with wGF are higher than those obtained with REF and fGF mixtures. Same trend in results was also observed in the literature for glass and other fibers (González et al., 2020; Małek et al., 2021). In the case of steel fibers, this is explained by the ability of the fibers to trap and retain more pores during preparation and because the fibers increase the stiffness of the mixture in a fresh state, leading to the retention of a larger number of larger pores (González et al., 2020; Mínguez et al., 2019). Higher values may also be caused by prolonged mixing time, i.e., more entrapped air.

Table 2. Fresh state properties for glass fibre reinforced mortars.

Mix ID	REF	fGF 6 – 2	wGF 5 - 2	fGF 12 - 6	wGF 10 - 6
Consistency [mm]	185/190	198/200	186/186	185/185	188/188
Density [g/dm3]	2199	2209	2137	2189	2025
Air content [%]	5.40	6.00	8.50	6.50	12.00
SP [% m_c]	0.40	0.42	0.46	0.42	0.62

3.2 Hardened state properties

The properties in the hardened state are presented below. The compressive strength was tested on the prisms after 28 days to confirm the properties of the high strength mortar, 50 – 100 MPa. The obtained values are shown in **Table *3***, representing the average strength value measured on 3 samples. The obtained results show a positive influence of both waste and factory-made fibers. The greater the amount and length of fibers, the greater the increase in strength in favor of

factory-made fibers. This may also be related to a higher proportion of pores in wGF mixes, resulting in lower compressive strength. Although the compressive strength values with waste fibers are lower compared to factory- made fibers, -9.5 % and -14 % for wGF5-2 and wGF10-6 respectively, the mixtures still meet the criterion for high strength category.

Table 3. Compressive strength values after 28 days on glass fiber reinforced cementitious materials.

Mix ID	REF	fGF 6 - 2	wGF 5 - 2	fGF 12 - 6	wGF 10 - 6
Compressive strength [MPa]	58.4 ± 2.4	71.2 ± 1.3	64.4 ± 1.6	76.6 ± 2.0	65.9 ± 2.2

Furthermore, the main parameters of pore morphology in all three types of mixtures were determined and discussed: porosity, pore-size distribution, pore shape and voids.

As can be seen from **Figure *1***, the total pore volume is highest for the waste fiber mixes, then factory made fibers and lowest for the reference mix. It can also be seen that the intrusion and extrusion curves do not coincide indicating a significant amount of mercury retained in the pore system. The difference is least with the reference mix, while the value increases with the use of glass fibers, factory made and waste. Both fiber lengths in fGF mixes had similar and slightly lower values than both fiber lengths in wGF. It is very likely that the higher mercury retention is due to the presence of 'ink-bottle' pores with narrow openings (Klemm & Sikora, 2013; Scrivener et al., 2018). As mentioned earlier, the presence of fibers in the fresh state leads to retention of a higher number of larger pores. Further hydration favored the formation of hydration products on their surface, which in turn led to the enclosing of the pores. Overall, the use of glass fibers resulted in an increase in the percentage of smaller pores, ink bottle pores, and overall porosity, with little to no change in pore size greater than $2 \cdot 10^3$ nm.

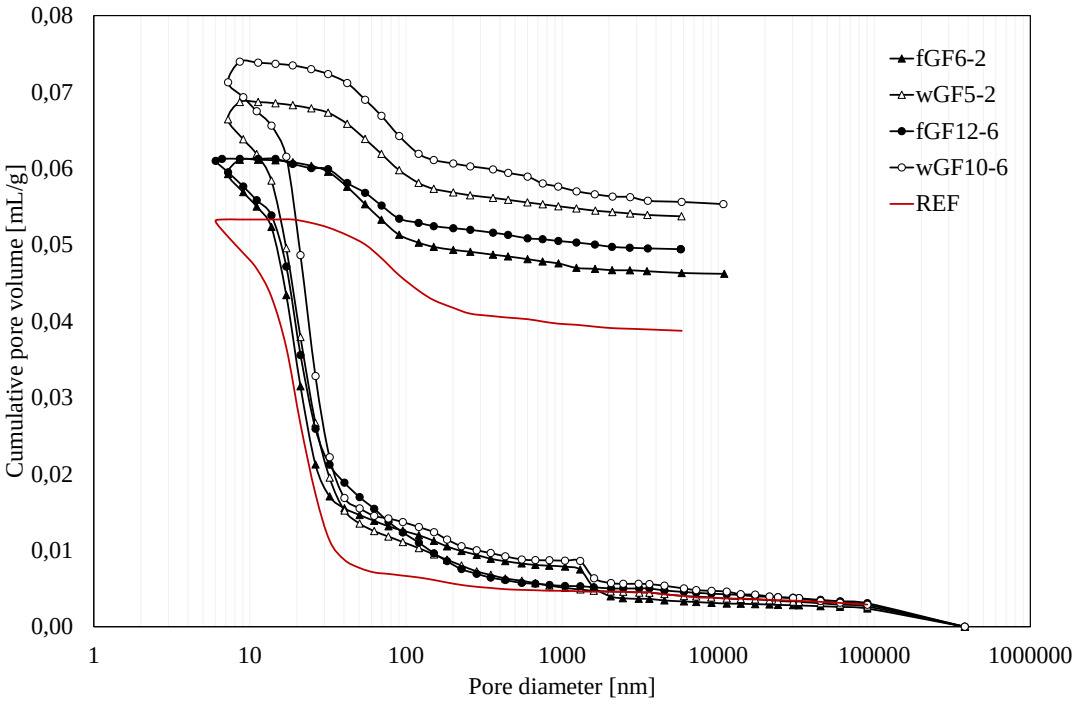

Figure 1. Cumulative pore volume of glass fiber reinforced mortar after 28 days.

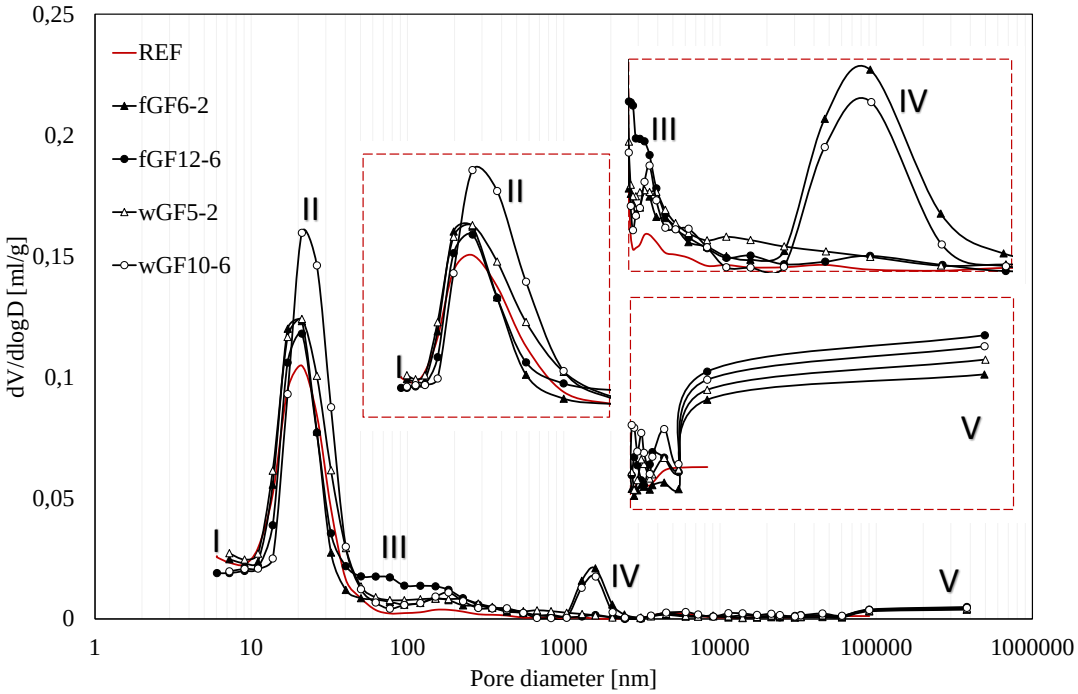

Figure 2. First derivatives for the cumulative curves after 28 days.

Due to the high mercury retention, the percentage of small pores may be questionable. When penetrating the 'ink-bottle' pores, a high pressure had to be applied (higher than for an equivalent pore size according to Washburn's model), suggesting a higher percentage of smaller pores than actually present (Klemm & Sikora, 2013).

Differential pore size distribution curves with characteristic peaks are shown in **Figure *2***. Peak I and peak II represent the inner and outer C-S-H gel pores, respectively (< 30 nm). Peak I remains unchanged as it represents the intrinsic nature of C-S-H, i.e., it is not affected by the fibers nor the amount of superplasticizer (Y. Zhang & Kong, 2014), while peak II was significantly higher for the wGF10-6 mix. From the results presented, it is clear that the use of fibers, both factory- made and waste, leads to higher values of gel and micro- capillary pores. In addition, peak III and peak IV, which represent mezzo- and macro- capillary pores, are shifted upwards for the mixes with fibers compared to the reference mix, indicating increased connectivity of capillary pores or a greater proportion of large pores (Y. Zhang & Kong, 2014). Peak V, which represents entrained air, is also slightly higher for the fiber mixes than for the reference.

The obtained total porosity and the mean pore diameter are shown in **Table *4***. From the comparison of the results presented, it can be seen that the addition of fibers affects the increase in porosity such that as the length and amount of fibers increase, the total porosity increases. The effect is more pronounced for 10 mm long fibers than for 5 mm long fibers.

The spatial distribution of pore shape and size determined by CT was processed on cube samples with dimensions X= 5501.4 µm, Y= 5501.4 µm, Z=7902.3 µm, with the XY plane shown in **Figure 3**. All images show pores larger than $7 \cdot 10^4$ nm, including macro- capillary pores and air pores (entrained and entrapped air). From the obtained images, it can be seen that the reference mixture has the highest volume percentage of larger pore diameter. This is

followed by the values from the mixtures with 5 mm and 10 mm long waste fibers and 6 mm and 12 mm long factory-made glass fibers, respectively.

Table 4. Pore morphology properties determined using MIP.

Mix ID	REF	fGF 6 - 2	wGF 5 - 2	fGF 12 - 6	wGF 10 - 6
Average pore diameter [nm]	19,42	22,87	23,31	19,74	25,67
Porosity [%]	12,622	13,470	13,048	16,065	16,567

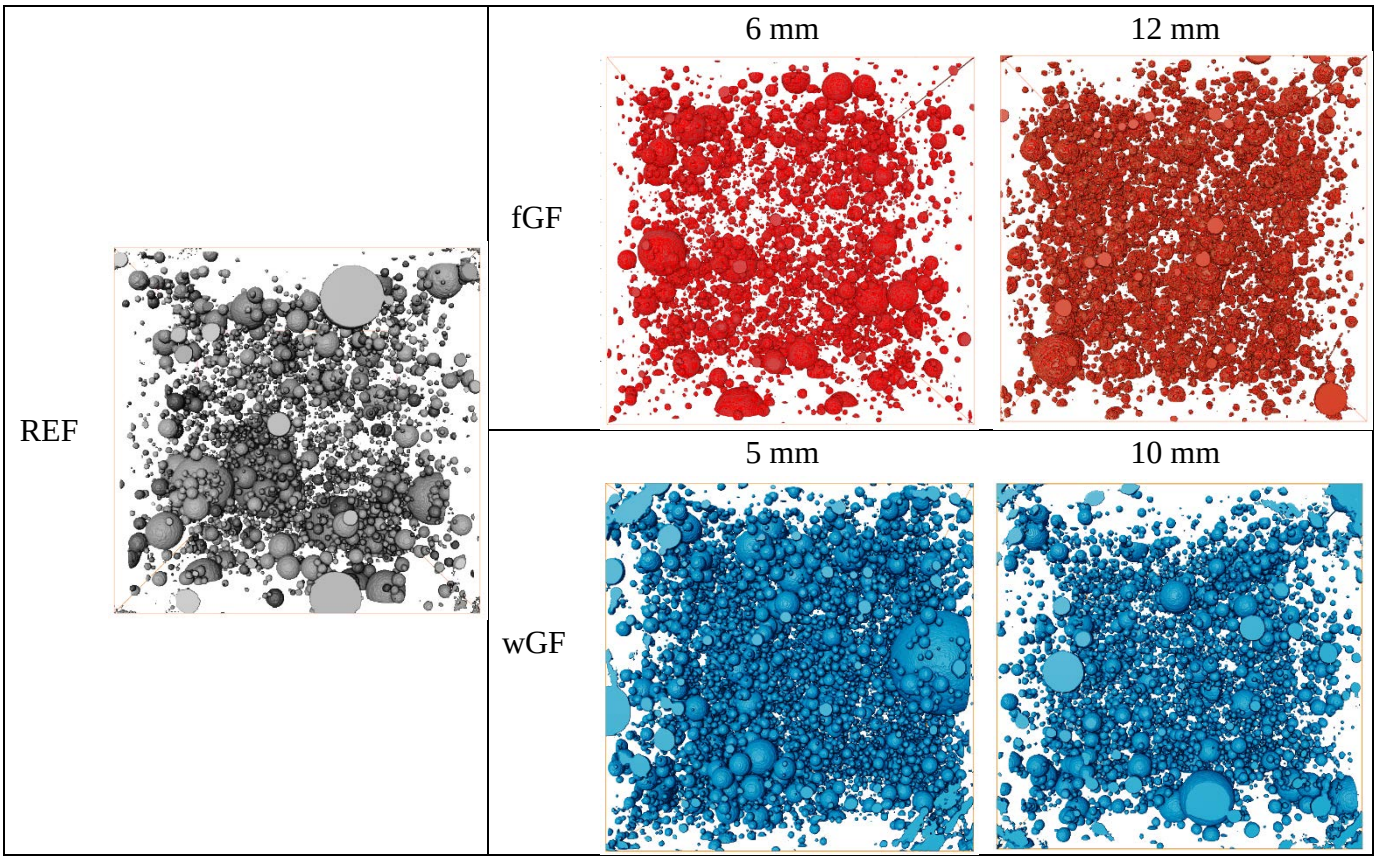

Figure 3. XY plane visualization using µCT (X= 5501.4 µm, Y= 5501.4 µm).

4 Conclusion

Based on the tests performed, the following conclusion can be drawn:

- Waste glass fibers, like factory-made fibers, decrease the consistency of the mixture i.e., a larger amount of superplasticizer is needed to achieve the same consistency values.
- Waste glass fibers increase the air content of the mixture but contribute to an increase in compressive strength compared to the reference mixture without fibers.
- Waste glass fibers increase the proportion of gel, capillary and entrained pores after 28 days compared to the reference mix without fibers.
- Waste glass fibers decrease the proportion of pores larger than $7 \cdot 10^4$ nm after 28 days compared to the reference mix without fibers.

Acknowledgements

The presented research is a part of the scientific project "Cementitious composites reinforced with waste fibres" – ReWire (UIP-2020-02-5242) and "Career Development of Young Researchers - Training of New Doctors of Science" (DOK-2021-02-4884) funded by the Croatian Science Foundation and carried out on Faculty of Civil Engineering, University of Zagreb.

ORCID

Katarina Didulica: https://orcid.org/0000-0003-1115-055X
Alenka Mauko Pranjić: https://orcid.org/0000-0002-9822-7806
Mateja Štefančić: https://orcid.org/0000-0002-7031-9426
Branka Mrduljaš: https://orcid.org/0000-0002-6550-6091
Ana Baričević: https://orcid.org/0000-0002-5779-9939

References

Ahmad, J., González-Lezcano, R. A., Majdi, A., Ben Kahla, N., Deifalla, A. F., & El-Shorbagy, M. A. (2022). Glass Fibers Reinforced Concrete: Overview on Mechanical, Durability and Microstructure Analysis. *Materials*, *15*(15), 1–23. https://doi.org/10.3390/ma15155111

Blazy, J., Blazy, R., & Drobiec, Ł. (2022). Glass Fiber Reinforced Concrete as a Durable and Enhanced Material for Structural and Architectural Elements in Smart City—A Review. *Materials*, *15*(8). https://doi.org/10.3390/ma15082754

Craipeau, T., Perrot, A., Toussaint, F., Huet, B., & Lecompte, T. (2021). Mortar pore pressure prediction during the first hours of cement hydration. *Cement and Concrete Composites*, *119*(March), 103998. https://doi.org/10.1016/j.cemconcomp.2021.103998

da Silva, J. L., & Lordsleem, A. C. (2021). Influence of mixer type and mixing time on the multipurpose mortars properties. *Case Studies in Construction Materials*, *15*(November 2020), e00562. https://doi.org/10.1016/j.cscm.2021.e00562

González, D. C., Rahman, M., Mínguez, J., Vicente, M. A., & Hindi, R. (2020). Influence of fibers and curing conditions on the pore morphology in plain and fiber-reinforced high-performance concrete through the use of computed tomography scan technology. *Applied Sciences (Switzerland)*, *10*(12). https://doi.org/10.3390/app10124286

Kang, S. H., Hong, S. G., & Moon, J. (2018). The effect of superabsorbent polymer on various scale of pore structure in ultra-high performance concrete. *Construction and Building Materials*, *172*, 29–40. https://doi.org/10.1016/j.conbuildmat.2018.03.193

Klemm, A. J., & Sikora, K. S. (2013). The effect of Superabsorbent Polymers (SAP) on microstructure and mechanical properties of fly ash cementitious mortars. *Construction and Building Materials*, *49*, 134–143. https://doi.org/10.1016/j.conbuildmat.2013.07.039

Małek, M., Jackowski, M., Łasica, W., Kadela, M., & Wachowski, M. (2021). Mechanical and material properties of mortar reinforced with glass fiber: An experimental study. *Materials*, *14*(3), 1–14. https://doi.org/10.3390/ma14030698

Mínguez, J., Vicente, M. A., & González, D. C. (2019). Pore morphology variation under ambient curing of plain and fiber-reinforced high performance mortar at an early age. *Construction and Building Materials*, *198*, 718–731. https://doi.org/10.1016/j.conbuildmat.2018.12.010

Scrivener, K., Snellings, R., & Lothenbach, B. (2018). A Practical Guide to Microstructural Analysis of Cementitious Materials. In *A Practical Guide to Microstructural Analysis of Cementitious Materials* (Vol. 62, Issue 10). https://doi.org/10.1201/b19074

Shi, C., Wu, Z., Xiao, J., Wang, D., Huang, Z., & Fang, Z. (2015). A review on ultra high performance concrete: Part I. Raw materials and mixture design. *Construction and Building Materials*, *101*, 741–751. https://doi.org/10.1016/j.conbuildmat.2015.10.088

Song, C., Hong, G., & Choi, S. (2020). Modeling autogenous shrinkage of hydrating cement paste by estimating the meniscus radius. *Construction and Building Materials*, *257*, 119521. https://doi.org/10.1016/j.conbuildmat.2020.119521

Tran, N. P., Gunasekara, C., Law, D. W., Houshyar, S., Setunge, S., & Cwirzen, A. (2021). A critical review on

drying shrinkage mitigation strategies in cement-based materials. *Journal of Building Engineering*, *38*(January), 102210. https://doi.org/10.1016/j.jobe.2021.102210

Wang, D., Shi, C., Wu, Z., Xiao, J., Huang, Z., & Fang, Z. (2015). A review on ultra high performance concrete: Part II. Hydration, microstructure and properties. *Construction and Building Materials*, *96*, 368–377. https://doi.org/10.1016/j.conbuildmat.2015.08.095

Wu, L., Farzadnia, N., Shi, C., Zhang, Z., & Wang, H. (2017). Autogenous shrinkage of high performance concrete: A review. *Construction and Building Materials*, *149*, 62–75. https://doi.org/10.1016/j.conbuildmat.2017.05.064

Xun, W., Wu, C., Leng, X., Li, J., Xin, D., & Li, Y. (2020). Effect of functional superplasticizers on concrete strength and pore structure. *Applied Sciences (Switzerland)*, *10*(10). https://doi.org/10.3390/app10103496

Yang, L., Shi, C., & Wu, Z. (2019). Mitigation techniques for autogenous shrinkage of ultra-high-performance concrete – A review. *Composites Part B: Engineering*, *178*(May), 107456. https://doi.org/10.1016/j.compositesb.2019.107456

Yu, Z., Zhao, Y., Ba, H., & Liu, M. (2021). Synergistic effects of ettringite-based expansive agent and polypropylene fiber on early-age anti-shrinkage and anti-cracking properties of mortars. *Journal of Building Engineering*, *39*(February), 102275. https://doi.org/10.1016/j.jobe.2021.102275

Zhang, J., Hou, D., & Han, Y. (2012). Micromechanical modeling on autogenous and drying shrinkages of concrete. *Construction and Building Materials*, *29*, 230–240. https://doi.org/10.1016/j.conbuildmat.2011.09.022

Zhang, Y., & Kong, X. (2014). Influences of PCE superplasticizer on the pore structure and the impermeability of hardened cementitious materials. *Journal of Advanced Concrete Technology*, *12*(10), 443–455. https://doi.org/10.3151/jact.12.443